Science of Sintering, **52** (2020) 283-298

doi:https://doi.org/10.2298/SOS2003283S

UDK: 669.018; 676.017.5; 532.74

The Inverted Hysteresis Loops and Exchange Bias Effects in Amorphous/Nanocrystalline $Fe_{72}Cu_1V_4Si_{15}B_8$ Ribbons at Room Temperature

Radoslav Surla[1], Nebojša Mitrović[1*)], Milica Vasić[2], Dragica Minić[2]

[1]Joint Laboratory for Advanced Materials, Section for Amorphous Systems, Faculty of Technical Sciences, University of Kragujevac, Svetog Save 65, 32 000 Čačak, Serbia

[2]Faculty of Physical Chemistry, University of Belgrade, Studentski trg 12-16, 11 000 Belgrade, Serbia

Abstract:

The influence of thermally induced microstructural transformations on magnetic properties of $Fe_{72}Cu_1V4Si_{15}B_8$ ribbon with combined amorphous/nanocrystalline structure is presented. The experiments showed that thermally induced structural changes are in correlation with the appearance of magnetic hysteresis, i.e. with inverted hysteresis loops (IHL) and exchange bias (EB) effects. It was found that the ratio of surface to volume of a ribbon sample have an influence on hysteresis loop appearance. The inverted hysteresis loops were observed for the 1.5 mm wide and 55 μm thick alloy samples shorter than 10 mm, but for the samples longer than 10 mm hysteresis loops were normal. With an increase of annealing temperature, a shift of the hysteresis loops measured at room temperature was noticed. The highest positive exchange bias field Heb was observed for the sample annealed at 723 K, together with the lowest magnetic field at which the changes from inverted to normal hysteresis loop occurred. Annealing at the temperature of 823 K resulted in negative Heb.

Keywords*: $Fe_{72}Cu_1V_4Si_{15}B_8$ ribbon; Amorphous/nanocrystalline structure; Inverted hysteresis loops; Exchange bias; Magnetic properties.*

1. Introduction

The nanocrystalline iron based alloys obtained from the starting amorphous precursors prepared by rapidly quenching technology are interesting topics in the field of the alloy research since they have excellent soft magnetic properties [1-4]. Moreover, in comparison with other iron based systems prepared by sintering technology [5-8], amorphous Fe-based ribbons have competitive functional properties. The Fe-Cu-M-Si-B (M = Cr, V, Mo, Nb, Ta, W) „FINEMET" type alloys with amorphous/nanocrystalline structure have been the subject of numerous scientific studies [9-13]. By selecting M-element different nanostructures were obtained. The experiments indicate that the best soft magnetic properties were attained in the alloys with the optimum α-Fe (Si) nanocrystalline grain size, which can be evolved by controlled annealing of the starting amorphous structure.

A recent investigation of thermally induced structural transformations of $Fe_{72}Cu_1V_4Si_{15}B_8$ alloy with combined amorphous/nanocrystalline structure showed that

***) Corresponding author:** nebojsa.mitrovic@ftn.kg.ac.rs (Dr. Nebojša Mitrović)

crystallization and recrystallization processes occurred in the temperature intervals from 740 K to 820 K and from 870 K to 930 K, respectively, during which α-Fe (Si) and iron-boron crystalline phases were formed [14]. The presence of traces of other phases in the annealed alloy samples, such as Fe_2VSi and ε-Cu, was also observed. Crystallization activation energy of α-Fe (Si) phase was determined lower in this alloy than in the other alloys of similar composition, which was explained by a large number of quenched-in nuclei in the as-prepared ribbon [14].
Thermal treatments resulted in transformation of $Fe_{23}B_6$ phase into Fe_2B phase while during recrystallization α-Fe (Si) phase becomes richer in Si. The relative magnetic permeability increases with the increase of temperature up to 773 K, but with further annealing it declines. Also, as the temperature of the treatment rises, the morphological changes on the surface affect its roughness which thereby becomes higher [14].

Inverted hysteresis loops effect

The study of magnetic hysteresis loops in ferromagnetic thin films where IHL was observed [15-17], is based on the assumption that there is a uniaxial anisotropy in the longitudinal direction which is mostly explained by the Stoner-Wohlfarth model [18]. An extended explanation was given by Arrot who studied ultra-thin magnetic films and found certain similarities in the magnetic properties of thin films with the nanoparticle systems [19, 20]. According to Arrot [20], thin film is like a single domain particle in the direction normal to the plane of the film.

Examining the METGLAS 2605SC alloy in the form of a plate, Tejedor et al. discovered different magnetization processes on the surface relative to the bulk of a material [21]. The origin of this behavior reflects different influences of demagnetization field on the surface and bulk of the ribbon. In some stages of the magnetizing process, vectors of the magnetization in surface M_{SF} and in bulk M_{BL} are oriented in opposite directions that can be followed by the appearance of IHL.

Shalyguina et al. found different magnetic properties on the surface and in the volume of heterogeneous (nanocrystalline/amorphous) $Fe_{81}Nb_7B_{12}$ ribbons prepared by a melt spinning method [22]. Changes of the magnetic properties induced by annealing are more pronounced in the vicinity of the surface than in the bulk of the alloy. Also, it was found that there different magnetic properties were indicated on the two sides of the ribbon due to the differences in residual stresses on the wheel side and the free side of the ribbon during production, as well as due to the differences in a surface morphology of these two sides. The IHL in the near-surface layers of this $Fe_{81}Nb_7B_{12}$ heterogeneous system is explained by a two-phase model, according to which two dissimilar phases (magnetically hard at the surface and magnetically soft in the volume) with uniaxial magnetic anisotropy exhibit antiferromagnetic exchange interaction.

Furthermore, IHL was found in the homogeneous EuS NP nanoparticle system. This is explained by the presence of a magnetically hard component formed by surface atoms and magnetic soft component which was created by atoms in the core of the nanoparticle system [23]. IHL was also observed in other magnetically non-homogeneous structures, where this phenomenon has been explained by the coexistence of a magnetically soft and magnetically hard component [24-28].

The total magnetic energy (per unit volume) of the two-phase model, according to the Stoner-Wohlfarth model, in the systems where IHL effect was observed, can be described by equation [23]:

$$E = K_h \cdot \sin^2\beta_h + K_s \cdot \sin^2\beta_{so} - M_h \cdot H \cdot \cos(\beta_h - \theta) - M_s \cdot H \cdot \cos(\beta_s - \theta) - J \cdot M_h \cdot M_s \cdot \cos(\beta_h - \beta_s) \quad (1)$$

where: K_h- the anisotropy constant of the hard component (that can be obtained from $2 \cdot K_h/M = H_c$) ; K_s- the anisotropy constant of the soft component; M_h - magnetization of the hard component; M_s - magnetization of the soft component; H- magnetic field; β_h – the angle between M_h and the easy axis of the hard component; β_s – the angle between M_s and the easy axis of the hard component; βs_0 – the angle between M_s and the easy axis of the soft component; θ- the angle between the applied field and the easy axis of the hard component and J - antiferromagnetic exchange coupling constant. The first two terms which present the uniaxial magnetic anisotropy energy are followed by two terms that present an expression for energy achieved by applying the external magnetic field (Zeeman energy). The last term presents the exchange interaction between the magnetically soft and hard components.

The total magnetization of the system can be given by [22]:

$$M = M_h \cdot cos(\beta_h - \theta) + M_s \cdot cos(\beta_s - \theta) \qquad (2)$$

Fig. 1 shows a model of the inverted hysteresis loop of the ribbon, which consists of two components (magnetically softer in the bulk and magnetically harder on the surface). Ascending and descending branches of the major hysteresis loop are obtained by the sum of magnetization of components according to equation (2). The saturation magnetization is significantly higher for the magnetically softer component, and therefore, exchange-coupled soft-hard biphasic system exhibit IHL effect.

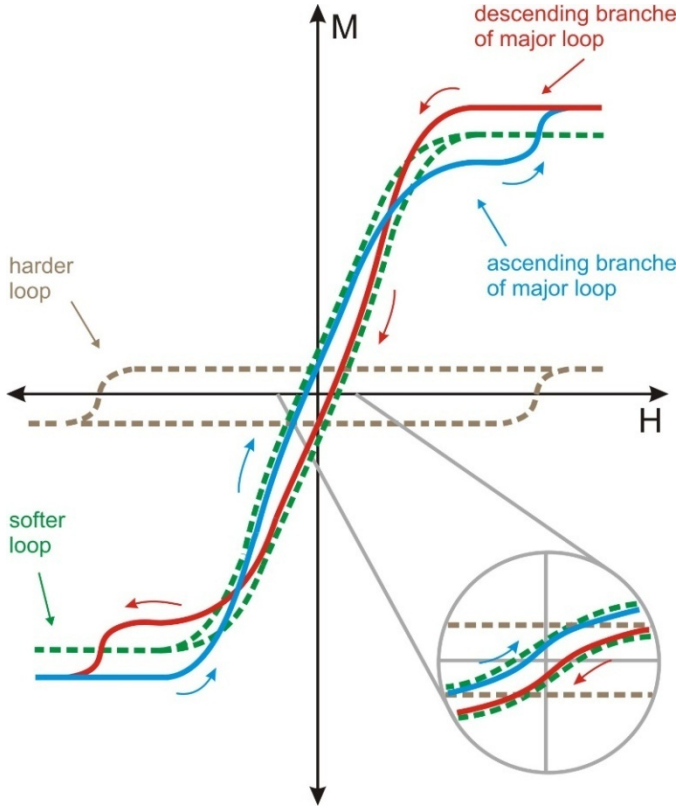

Fig. 1. Inverted hysteresis loop of soft-hard exchange-coupled biphasic magnetic system.

1.2. Exchange bias effect

Meiklejohn and Bean discovered the Exchange bias effect in 1956 [29] and named it with the new type of magnetic anisotropy (hysteresis loop shifts away from the H = 0). The

effect was found on fine particles of cobalt which were made by electrodeposition of cobalt into mercury. The electrodeposition of cobalt was followed by oxidization in order to produce cobaltous oxide shell. During cooling, CoO at the Neel temperature (293 K) has transition from the paramagnetic to the antiferromagnetic state and the system is characterized by the interaction of ferromagnetic Co and antiferromagnetic CoO. If saturating magnetic field is applied during cooling to 77 K, hysteresis loop shifts to the left, i.e. a negative EB effect (NEB) occurs. A positive EB (PEB) was found in the FeF_2-Fe bilayer system [30], which was obtained by applying a large magnetic field during cooling through the Neel temperature. Therefore, the EB effect is explained by the existence of an antiferromagnetic exchange between the various magnetic components resulting in a shift of the hysteresis loop. The effect was first found in a combination of ferromagnetic/antiferromagnetic (FM/AFM) system [29]. However, the combinations of antiferromagnetic/ferrimagnetic (AFM/ferri), and ferromagnetic/ferrimagnetic (FM/ferri) components were later examined [31]. In the combination of a soft/hard Fe/Co spring magnet system prepared by pinning magnetic field influence, PEB is observed even at the room temperature [32]. Extensive theoretical background supported by experimental results on exchange bias/exchange anisotropy was published [33-36].

The magnetic energy (per unit area) of two-phase model regarding the real Meiklejohn and Bean model where EB was observed can be described by equation [37]:

$$E_A = K_F \cdot t_F \cdot \sin^2\beta + K_{AF} \cdot t_{AF} \cdot \sin^2\alpha - \mu_0 \cdot H \cdot M_F \cdot t_F \cdot \cos(\theta^* - \beta) - J_{eb} \cdot \cos(\beta - \alpha) \quad (3)$$

where M_F - saturation magnetization of the ferromagnetic component, H - magnetic field, α - the angle between the magnetic moment of the antiferromagnetic component M_{AF} and easy axis, β - the angle between the magnetic moment of the ferromagnetic component M_F and easy axis, θ^*- the angle between the magnetic field H and easy axis, K_{AF} and K_F are magnetic anisotropy coefficient of the antiferromagnetic and ferromagnetic components respectively, t_F and t_{AF} are thicknesses of the ferromagnetic and antiferromagnetic components respectively, and J_{eb} – exchange energy between ferromagnetic and antiferromagnetic components. The first two terms represent uniaxial magnetic anisotropy energy; the next term is an expression for Zeeman energy, while the last term represents an expression for the antiferromagnetic exchange. For an ideal model (α = 0) the antiferromagnetic anisotropy energy disappears and energy is expressed by the next equation:

$$E_A = K_F \cdot t_F \cdot \sin^2\beta - \mu_0 \cdot H \cdot M_F \cdot t_F \cdot \cos(-\beta) - J_{eb} \cdot \cos\beta \quad (4)$$

Fig. 2 shows the shift of the hysteresis loop where unlike the classical loop, a new term is introduced, exchange bias field (H_{eb}), which defines the loop displacement.

The coercive field is calculated from the intersection points of the hysteresis loop with H axis (H_{c1} and H_{c2}). The coercivity H_c of the loop and the loop displacement H_{eb} can be calculated according to the following equations [37]:

$$H_c = |-H_{c1} + H_{c2}| / 2, \quad H_{eb} = (H_{c1} + H_{c2})/2 \quad (5)$$

For both models (S-W and M-B), it is inherent that the total magnetization energy is made of: (i) – the energy of anisotropy, (ii) - Zeeman energy and (iii) – the energy of antiferromagnetic exchange.

The aim of this research is to investigate the influence of thermally induced structural changes on magnetic properties of $Fe_{72}Cu_1V_4Si_{15}B_8$ ribbons and therefore on the inverted hysteresis loops (IHL) and the exchange bias (EB) effects that appeared. The evolution of amorphous/nanocrystalline structure accompanied with the appearance of EB effect as well as

the influence of sample length on IHL effect, was studied. The investigated FeCuVSiB alloy ribbons possess curious properties as a magnetoimpedance MI - sensing element [38].

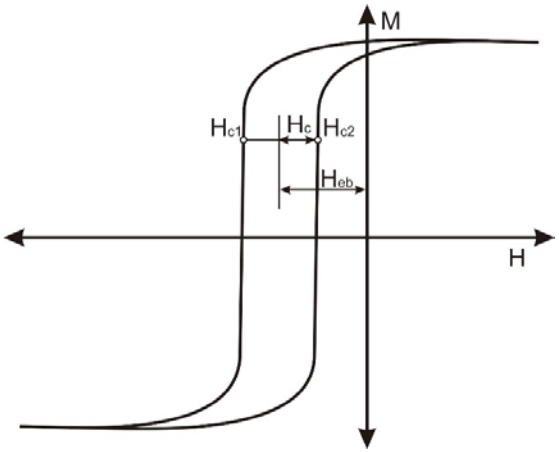

Fig. 2. The shift of hysteresis loop due to the exchange of energy between different components, with marked characteristic points H_c, H_{c1}, H_{c2} and H_{eb} [38].

2. Materials and Experimental Procedures

This research paper aims to analyze the ribbons of metastable alloy $Fe_{72}Cu_1V_4Si_{15}B_8$, with a thickness of about 55 μm and width of 1.5 mm obtained by melt-spinning method.

X-ray diffraction patterns were recorded using a Rigaku SmartLab diffractometer with a Cu $_{K\alpha}$ radiation source at room temperature. The obtained XRD patterns were analyzed by means of the Maud software [39] and databases PDF-2 [40] and ICSD [41]. The observed crystalline phases were identified according to the cards No. PDF#35-0519, PDF#75-1062 and ICSD#54786. Williamson-Hall method [42] was applied to get the values of average crystallite size.

Magnetic measurements were performed at room temperature by a Faraday balance as well as by SQUID device. In both cases, the orientation of the applied magnetic field was parallel to the length of the ribbon.

The Faraday balance was used to observe the dependence of the normalized magnetization $M(H_{ex})/M_{max}$ for the as-cast alloy samples of different lengths 4 mm, 6 mm, 10 mm, 15 mm , 20 mm and 29 mm. Sample thickness and width were the same for all studied samples (55 μm and 1.5 mm, respectively). External magnetic field H_{ex} varied from 0 to 10.695 kA/m with the step of 0.345 kA/m. The magnetic force (F) was measured by analytical balance OHAUS, model EP4102CM with 10^{-6} N sensitivity.

The change of magnetic force $\Delta F(H_{ex}) = \Delta m(H_{ex}) \cdot g$ was obtained under the external magnetic field influence on the ribbon sample and normalized magnetization was defined by:

$$M(H_{ex})/M_{max} = \Delta m(H_{ex})/\Delta m_{max} \qquad (6)$$

where $\Delta m_{max} = m(H_{max}) - m(0)$ is measured at $H_{max} = 10.695$ kA/m.

The static hysteresis loops were measured at room temperature with an MPMS-XL5 Quantum Design SQUID device, in the magnetic field intensity up to 5032 Oe (400.434 kA/m) in both directions. The measurement was performed with increasing measuring step: from zero the step was 10 Oe (0.796 kA/m) but after magnetic saturation (above 300 Oe) the

step was 500 Oe (39.789 kA/m). Measurements were performed on a 6 mm long as-cast sample and samples annealed at different temperatures 723, 773 and 823 K, for one hour.

3. Results and Discussion

3.1 Structural analysis

The as-cast sample of the $Fe_{72}Cu_1V_4Si_{15}B_8$ alloy contains both amorphous and crystalline phases, as indicated by the broad halo and narrow diffraction peaks in XRD patterns given in Fig. 3a.

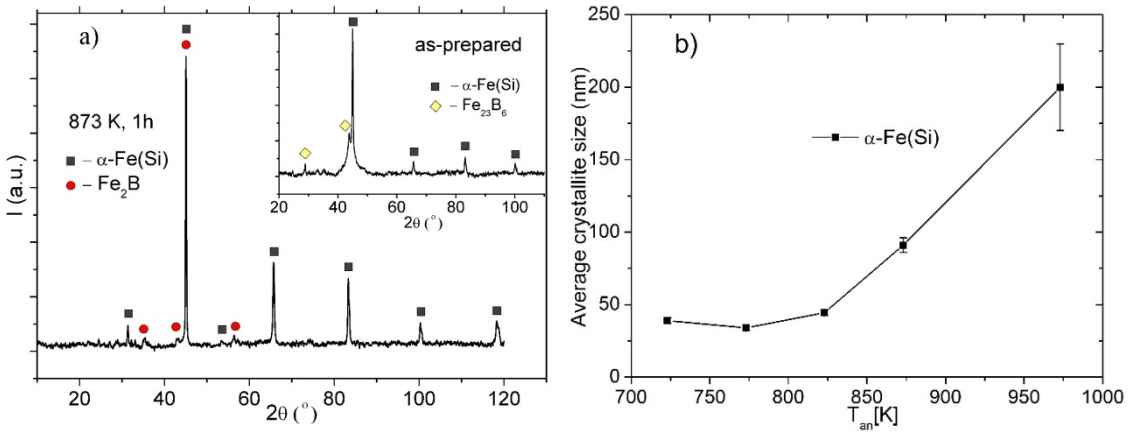

Fig. 3. a) XRD patterns of the sample annealed at 873 K with the inset showing the XRD of as-cast alloy; and b) average crystallite size of the α-Fe (Si) phase depending on the annealing temperature.

Thermal treatment of the alloy at different temperatures for 60 min provokes structural transformations starting from 723 K [14], see Tab. I.

Tab. I Phases present in the as-cast and thermally treated alloy samples [14].

Sample	Phases
As-cast	Amorphous, α-Fe(Si), $Fe_{23}B_6$
Annealed at 723 K for 60 min	Amorphous, α-Fe(Si), $Fe_{23}B_6$, Fe_2B
Annealed at 773 K for 60 min	Amorphous, α-Fe(Si), $Fe_{23}B_6$, Fe_2B
Annealed at 823 K for 60 min	α-Fe(Si), Fe_2B
Annealed at 873 K for 60 min	α-Fe(Si), Fe_2B
Annealed at 973 K for 60 min	α-Fe(Si), Fe_2B

Besides the changes in weight fraction of the phases already present in the as-cast alloy, after annealing at 723 K Fe_2B phase also begins to crystallize. The $Fe_{23}B_6$ phase completely disappears at higher annealing temperatures ($T_{an} \geq 823$ K), so that in an entirely crystalline alloy only α-Fe (Si) and Fe_2B phases can be found. The average crystallite size of the α-Fe (Si) exhibits weak changes up to annealing temperature of 823 K (see Fig. 3b). Higher annealing temperatures stimulate a sudden growth, which can be correlated with the presence of vanadium in the alloy [9, 14].

3.2 Magnetic measurements by a Faraday balance

It is generally considered that, the ferromagnetic thin ribbons, exhibit a different magnetic behavior in the near-surface layer and in the bulk of the ribbon [21, 22]. The

influence of the length of the as-cast $Fe_{72}Cu_1V_4Si_{15}B_8$ ribbon samples on its magnetic properties was analyzed using a Faraday balance. The length differences change the surface-to-volume ratio of the sample, influencing the magnetization changes. This method was used to observe the trend of hysteresis loop changes in the vicinity of saturation (magnetic field up to the 10.7 kA/m).

In Fig. 4, the diagrams a), b) and c) show the IHL trend for the ribbon length of 4 mm, 6 mm, and 10 mm. This behavior was not found for the samples longer than 10 mm (Fig. 4d, 4e, 4f). For samples of 6 mm and 10 mm length, points when the hysteresis loop changes from normal to inverted trend were observed (for instance 6.7 kA/m is the intersection of descending and ascending curves of 10 mm sample).

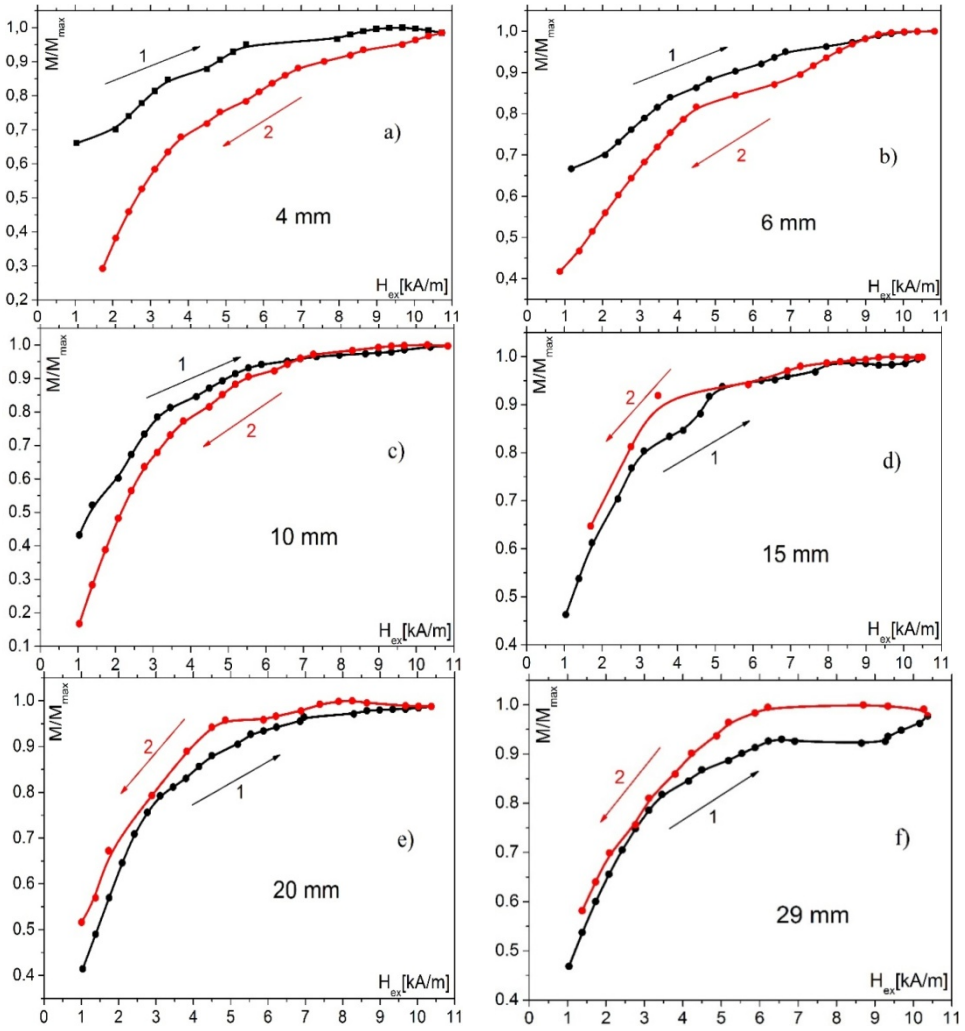

Fig. 4. Influence of magnetic field H (A/m) on normalized magnetization (M/M_{max}) for as-cast $Fe_{72}Cu_1V_4Si_{15}B_8$ ribbon samples of different length: a) 4 mm, b) 6 mm, c) 10 mm, d) 15 mm, e) 20 mm and f) 29 mm.

Faraday's method has unequivocally shown that the inverted hysteresis loops of the investigated $Fe_{72}Cu_1V_4Si_{15}B_8$ samples are dependent upon the length of the ribbons. The change of the length of the ribbons is followed by the changes of surface to volume ratio of a ribbon and therefore by the changes of magnetic energy (the last term in equation (1) - antiferromagnetic exchange interaction between the surface layer and the bulk; surface layer as a magnetically harder component and bulk as a magnetically softer component [21-23]).

3.3 SQUID magnetic measurements

By recording the magnetic hysteresis of the $Fe_{72}Cu_1V_4Si_{15}B_8$ ribbons with SQUID device at room temperature, two effects were detected: inverted hysteresis loops (IHL) and exchange bias (EB). Fig. 5 shows the dependence of magnetic moment *m* (emu) on the applied magnetic field. The inverted hysteresis loops were observed in all the studied 6 mm-long ribbon samples (as-prepared and annealed at 723 K, 773 K and 823 K for 1h), in line with the Faraday's balance results regarding the sample length. At high negative magnetic field (about H ≈ - 2000 Oe), it was observed that magnetic moment changes from inverted into normal, i.e. orientation toward the field direction (inserts on the left side in the Fig. 5).

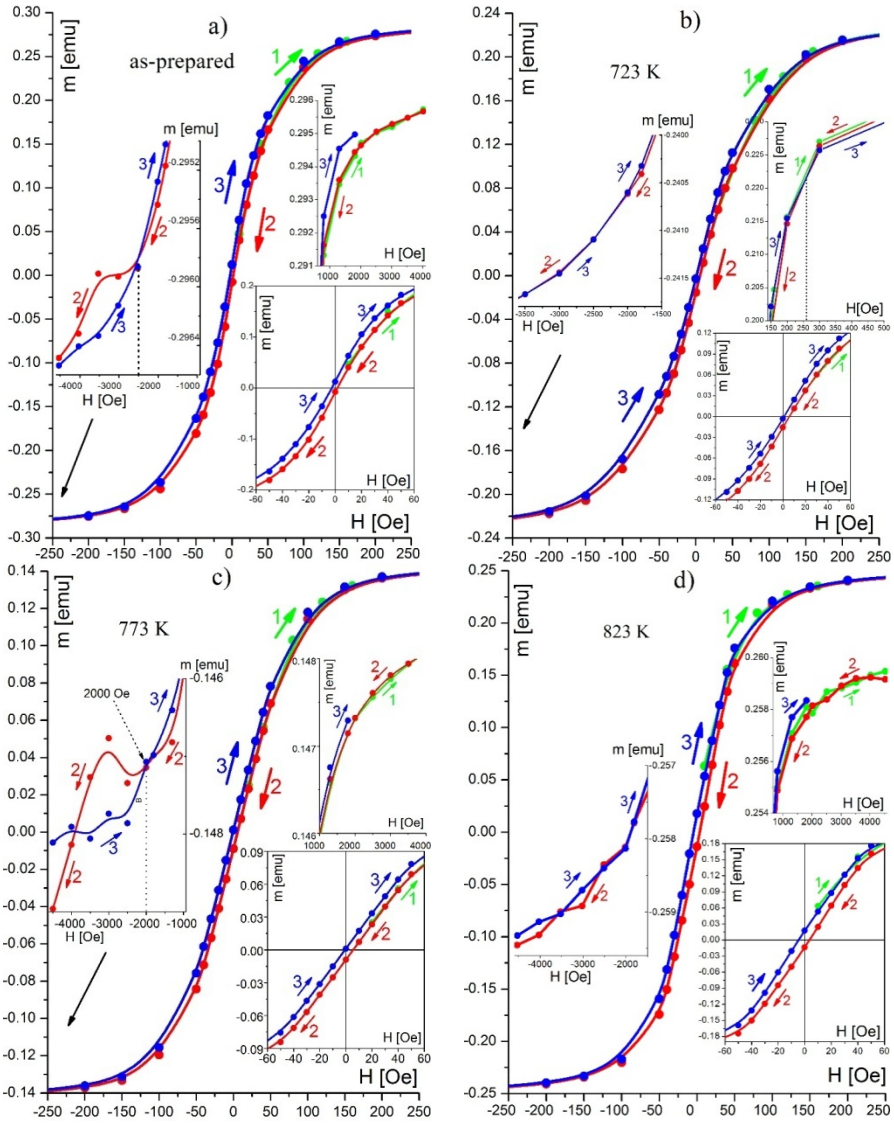

Fig. 5. Dependence of the magnetic moment on the magnetic field of $Fe_{72}Cu_1V_4Si_{15}B_8$: a) as-prepared ribbon sample and samples annealed at temperature b) 723 K, c) 773 K and d) 823 K.

Furthermore, magnetic properties of the $Fe_{72}Cu_1V_4Si_{15}B_8$ alloy exhibits changes after annealing caused by thermally induced structural transformations. Namely, the SQUID results show that the mass saturation magnetization M_S (emu/g) increases with the increase in

annealing temperature up to 773 K, while the annealing at higher temperature results in its decline (Fig. 6 and Fig. 8a). The formation of magnetic nanocrystalline α-Fe (Si) particles in the amorphous matrix causes an increase in saturation magnetization at lower annealing temperatures. At annealing temperatures higher than 773 K, with further progress of crystallization, non-magnetic B atoms are accumulated along the α-Fe (Si) grain boundaries in larger amounts, reducing the ferromagnetic exchange interaction among the α-Fe (Si) crystals [43]. However, the structural characteristics at higher annealing temperatures, including a larger fraction of crystalline material in the alloy, hinder the movement of magnetic domain walls additionally diminishing the magnetization value.

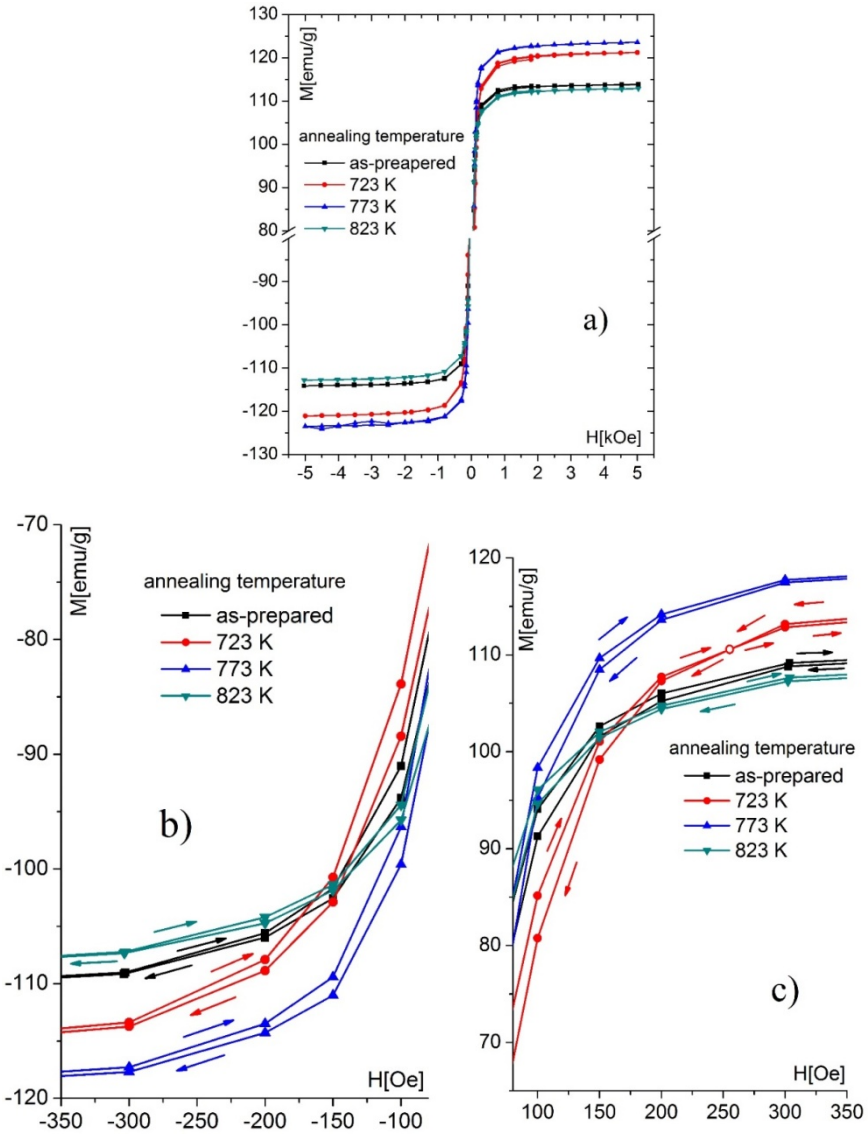

Fig. 6. The influence of annealing on magnetic hysteresis loops for the $Fe_{72}Cu_1V_4Si_{15}B_8$ as-prepared ribbon and samples annealed at temperatures 723 K, 773 K and 823 K: a) whole view, b) view in negative magnetic field region and c) view in positive magnetic field region.

On the other hand, coercive field H_c exhibits a constant increase with an increase of annealing temperature (Fig. 7 and Fig. 8c). This growing trend of H_c can be explained by the

progress of crystallization process with an increase in annealing temperature. As previously mentioned, during the crystallization, the α-Fe (Si) crystals, as well as the boride ones are formed. It is considered that the nanocrystal size, that is lower than the magnetic exchange length, significantly diminishes the contribution of magnetocrystalline anisotropy of the nanocrystals to the overall magnetic anisotropy of the material [2, 44], which is directly related to coercivity.

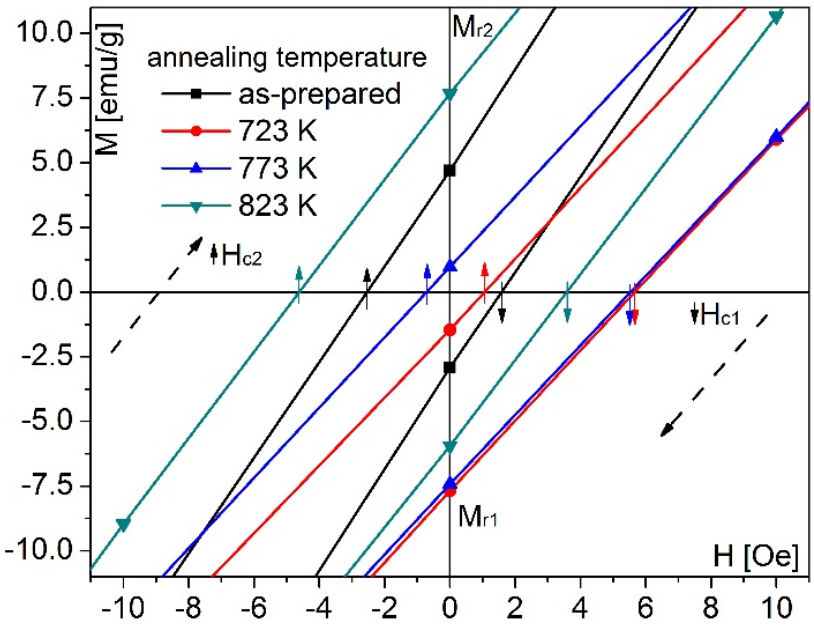

Fig. 7. Hysteresis loops near H_C for $Fe_{72}Cu_1V_4Si_{15}B_8$ as-prepared ribbon and samples annealed at temperatures 723 K, 773 K and 823 K

The ferromagnetic exchange length for Fe-based alloys is believed to be 20 nm - 40 nm [45]. In the temperature interval up to 823 K, the average crystallite size of the dominant phase, α-Fe (Si), slightly increases with the progress of crystallization, from about 40 nm to 44 nm (see Fig. 3b). This increase can affect the average anisotropy, as the coercivity is proportional to the sixth power of the grain size [43]. The formation of small amounts of boride phase in this system additionally contributes to deterioration of the soft magnetic properties due to large magnetocrystalline anisotropy constant. Moreover, the structural changes induced by annealing lead to the change of the domain structure of material, which is reflected in the movement of the easy axis of magnetization, i.e. to the changes in magnetic anisotropy [45].

In most cases, exchange bias (EB) has been found below the Neil temperature, under which the antiferromagnetic exchange behavior occurs. At room temperature, EB effect was found in a two-layer film that consisted of a magnetically soft and a magnetically hard ferromagnetic layer, but with a pinning field applied [32]. Exchange bias in the $Fe_{72}Cu_1V_4Si_{15}B_8$ alloy was found at room temperature for all investigated samples (as-cast and annealed at 723 K, 773 K and 823 K), but without the application of the cooling (pinning) field (Fig. 7 and Fig. 8). The effect can be explained by the antiferromagnetic exchange of the surface layer and bulk of the material that is also the origin of IHL (equations (1) and (3)).

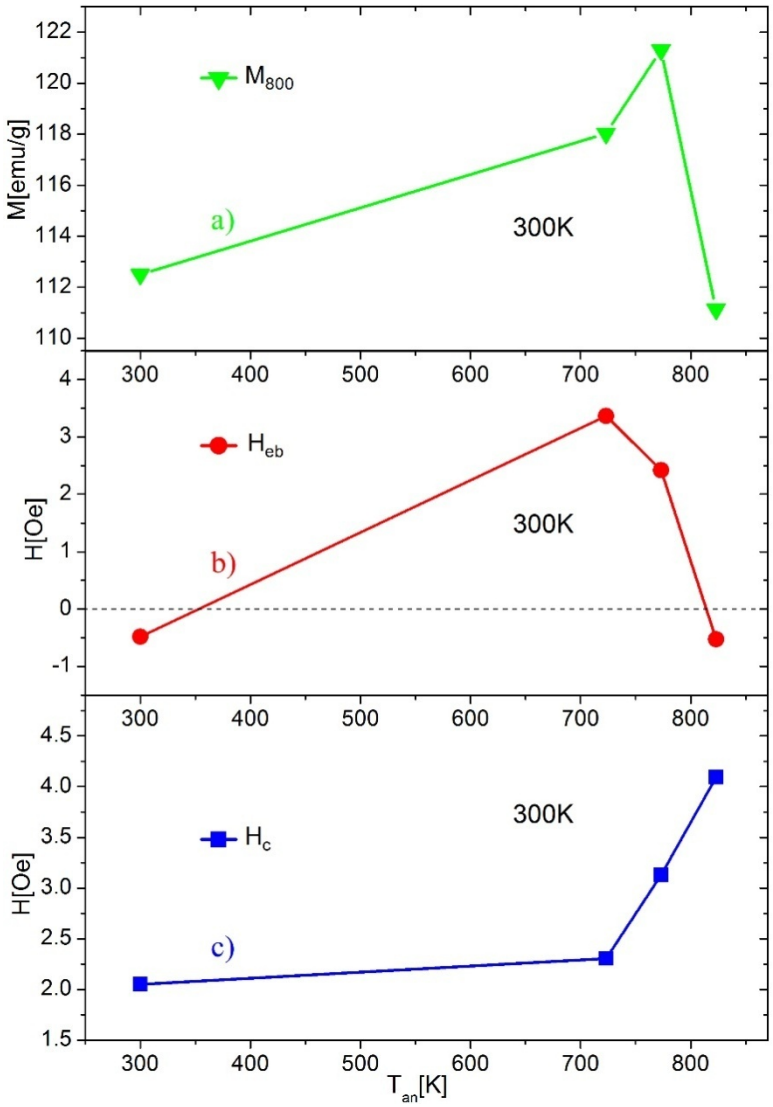

Fig. 8. Dependence of **a)** mas magnetization M_{800}, **b)** exchange bias field H_{eb} and **c)** coercive field $H_{c,}$ measured at 300 K after annealing at temperature T_{an}.

By analyzing the results of the magnetic measurements (Fig. 7) in the as-cast alloy H_{eb} is negative - NEB (see Tab. II). Annealing at 723 K and 773 K was followed by the shift of the hysteresis loop to the right, i.e. to the positive EB effect (PEB).

Tab. II EB magnetic properties of the investigated samples.

T (K)	**H_{c1}** (Oe)	**H_{c2}** (Oe)	**H_c** (Oe)	**H_{eb}** (Oe)	**M_{r1}** (emu/g)	**M_{r2}** (emu/g)	**M** (for 800 Oe)
as-cast	1,57	-2,53	2,05	-0,48	-2,92	4,7	112,5
723	5,67	1,06	2,305	3,365	-7,68	-1,46	118,03
773	5,55	-0,71	3,13	2,42	-7,43	0,97	121,3
823	3,57	-4,62	4,095	-0,525	-5,94	7,68	111,14

For the sample annealed at temperature of 723 K, the highest H_{eb} value, as well as the largest hysteresis loop displacement to the right was recorded. This can be associated with an increase in saturation magnetization, M_s, joint with a minimal increase of magnetic anisotropy; which was thereby, followed by a small increase in H_c. This indicated a larger influence of the magnetic soft component (due to enhanced magnetic moment) on antiferromagnetic exchange. Further increase of annealing temperature up to 773 K, causes both a slight increase of M_s, and an increase of H_c, and due to the reduced influence of the magnetically soft component, the resulting hysteresis loop shifts to the left. EB remains positive due to still dominant influence of magnetically soft component in antiferromagnetic exchange. After annealing at 823 K, there was an evident decrease of M_s, while H_c still continues to grow, which significantly contributes to the hysteresis loop displacement to the left, i.e. EB became negative and $|H_{eb823K}| > |H_{eb300K}|$).

Also, the correlations of IHL and EB effect were detected. Namely, after annealing at 723 K, the highest value of positive H_{eb} was observed, as well as the lowest value of the magnetic field where the hysteresis loop exhibits a transition from inverted into normal direction (about 250 Oe, see Fig. 6c).

4. Conclusion

In amorphous/nanocrystalline ribbon of $Fe_{72}Cu_1V_4Si_{15}B_8$ („FINEMENT type“ alloy Fe-Cu-**M**-Si-B, **M**=V) obtained by melt spinning technique, both the IHL and the EB effects at room temperature were found. IHL trend was observed for the as-cast ribbons with length of 4 mm, 6 mm and 10 mm. In the as-cast ribbon H_{eb} is negative as hysteresis loop was displaced to the left in relation to the H=0 axis.

Depending on annealing temperature, amorphous matrix with α-Fe (Si), $Fe_{23}B_6$ and Fe_2B nanocrystalline phases coexists. The structural changes induced by annealing up to 773 K have a positive influence on M_s, which is linked to the stress relief and transformation of the residual amorphous matrix into nanocrystalline phase, where the α-Fe (Si) phase is more abundant and configuration of magnetic domains is more favorable (domain wall movement is higher). Further increase of T_{an} results in the increase of the content of boride phases and deteriorates soft magnetic properties of the alloy. For T_{an} > 773 K, transformation of $Fe_{23}B_6$ into Fe_2B and growth of crystallites, reduce M_s as well as magnetic domain wall movement.

By annealing the 6 mm long ribbons, IHL effect is observed in all of the annealed samples due to antiferromagnetic exchange between the surface (magnetically harder component) and bulk (magnetically softer component). Positive H_{eb} occurred and maximum shift to the right was recorded after annealing at 723 K. On the other hand, significant hysteresis loop displacement to the left was observed after annealing at 823 K, i.e. EB became negative and $|H_{eb823K}| > |H_{eb300K}|$).

Acknowledgments

The authors would like to thank Dr. Vladan Kusigerski from Department of Theoretical Physics and Condensed Matter Physics of Vinča Institute – University of Belgrade for SQUID experiments. This study was supported by the Ministry of Education, Science and Technological Development of the Republic of Serbia, and these results are parts of the Grant No. 451-03-68/2020-14/200132 of University of Kragujevac - Faculty of Technical Sciences Čačak, and Grant No. 451-03-68/2020-14/200146 of University of Belgrade - Faculty of Physical Chemistry.

5. References

1. G. Herzer, Nanocrystalline soft magnetic alloys, in K. H. J. Buschow (Eds.), Handbook of Magnetic Materials, 1997, 415-462.
2. T. Kulik, Nanocrystallization of metallic glasses, J. Non-Cryst. Solids, 287 (2001) 145-161.
3. M. Stoica, R. Li, S. Roth, J. Eckert, G. Vaughan and A. R. Yavari, $[(Fe_{0.5}Co_{0.5})_{0.75}B_{0.20}Si_{0.05}]_{96}Nb_4$ metallic glasses with small Cu additions, Metal. Mater. Trans. A, 42A (2011) 1476-1480.
4. N. Mitrović, S. Djukić and S. Djurić, Crystallization of the Fe-Cu-M-Si-B (M = Nb, V) amorphous alloys by direct-current Joule heating, IEEE T. Magn. 36 (2000) 3858-3862.
5. R. Hasegawa, Advances in amorphous and nanocrystalline materials, J. Mag. Mag. Mater. 324 (2012) 3555-3557.
6. M. Tenerowicz-Zaba and M. Sulowski, A comparison of mechanical properties and microstructures of PM steels with chemical compositions Fe - (1-3) % Mn - 0.8 % C, Sci. Sinter. 50 (2018) 457-466.
7. A. Makino, T. Kubota, K. Yubuta, A. Inoue, A. Urata, H. Matsumoto and S. Yoshida, Low core losses and magnetic properties of $Fe_{85\text{-}86}Si_{1\text{-}2}B_8P_4Cu_1$ nanocrystalline alloys with high B for power applications (invited), J. Appl. Phys. 109 (2011) 07A303.
8. B. Nedeljković, N. Mitrović, J. Orelj, N. Obradović and V. Pavlović, Characterization of FeCoV alloy processed by PIM/MIM route, Sci. Sinter. 49 (2017) 299-309.
9. Y. Yoshizawa and K. Yamauchi, Magnetic properties of Fe-Cu-M-Si-B (M = Cr, V, Mo, Nb, Ta, W alloys, Mat. Sci. Eng. A133 (1991) 176-179.
10. P. Duhaj, P. Švec, D. Janičković, I. Matko and M. Hlaisnik, Structure and magnetic properties of the Finemet alloy $Fe_{73}Cu_lNb_3Si_{13.5}B_{9.5}$, Mat. Sci. Eng. B14 (1991) 357-364.
11. L. K. Varga, E. Bakos, L. F. Kiss and I. Bakonyi, The kinetics of amorphous-nanocrystalline transformation for a Finemet alloy, Mat. Sci. Eng. A179/A180 (1994) 567-571.
12. N. Mitrović, Magnetoresistance of the $Fe_{72}Cu_1V_3Si_{16}B_8$ amorphous alloy annealed by direct current Joule heating, J. Mag. Mag. Mater. 262 (2003) 302-307.
13. G. Pozo, Lopez, L. M. Fabietti, A. M. Condo and S. E. Urreta, Microstructure and soft magnetic properties of Finemet-type ribbons obtained by twin-roller melt-spinning, J. Mag. Mag. Mater. 322 (2010) 3088-3093.
14. M. Vasić, R. Surla, D. Minić, Lj. Radović, N. Mitrović, A. Maričić and D. Minić, Thermally induced microstructural transformations of $Fe_{72}Si_{15}B_8V_4Cu_1$ alloy, Metal. Mater. Tran. A, 48a (2017) 4393-4402.
15. S. M. Valvidares, J. I. Martin, L. M. Alvarez-Prado, D. Pain, O. Acher, G. Suran and J. M. Alameda, Inverted hysteresis loops in annealed Co–Nb–Zr and Co–Fe–Mo–Si–B amorphous thin films, J. Mag. Mag. Mater. 242–245 (2002) 169-172.
16. D. Y. Kim, C. G. Kim, C-O. Kim, S. S. Yoon, M. Naka, M. Tsunoda and M. Takahashi, Inverted hysteresis loops in annealed Co–Nb–Zr and Co–Fe–Mo–Si–B amorphous thin films, J. Mag. Mag. Mater. 304 (2006) e356-e358.

17. N. D. Ha, T. S. Yoon, E. Gan'shina, M. H. Phan, C. G. Kim and C. O. Kim, Observation of reversed hysteresis loops and negative coercivity in CoFeAlO magnetic thin films, J. Mag. Mag. Mater. 295 (2005) 126-131.
18. E. C. Stoner and E. P. Wohlfarth, A Mechanism of magnetic hysteresis in heterogeneous alloys, Phil. Trans. R. Soc. Lon. A, 240 (1948) 599-642.
19. A. S. Arrott and B. Heinrich, Phenomenology of anisotropy in the ferromagnetism of ultrathin films, J. Mag. Mag. Mater. 93 (1991) 571-586.
20. A. S. Arrott, Origins of hysteresis in ultrathin films, in: A. Hernando (Eds.), Nanomagnetism, NATO ASI, Sprin. Neth. (1993) 73-85.
21. M. Tejedor, H. Rubio and A. Fernandez, Origin of inverted-in-sense and constricted near-surface hysteresis loops of magnetic plates, Appl. Phys. Lett. 55 (1989) 1920-1922.
22. E. E. Shalyguina, I. Škorvánek, P. Švec, V. A. Melnikov and N. M. Abrosimova, Inverted near-surface hysteresis loops in heterogeneous (nanocrystalline/amorphous) $Fe_{81}Nb_7B_{12}$ alloys, J. Exp. Theor. Phys. 99 (2004) 544-551.
23. S. Gu, W. He, M. Zhang, T. Zhuang, Y. Jin, H. El, Bidweihy, Y. Mao, J. H. Dickerson, M. J. Wagner, E. D. Torre and L. H. Bennett, Physical justification for negative remanent magnetization in homogeneous nanoparticles, Sci. Rep. 4 (2014) 1-7.
24. M. J. O'Sheaand and A. L. Al-Sharif, Inverted hysteresis in magnetic systems with interface exchange, J. Appl. Phys. 75 (1994) 6673-6675.
25. X. Yan and Y. Xu, Negative remanence in magnetic nanostructures, J. Appl. Phys. 79 (1996) 6013–6015.
26. S. Ohkoshi, T. Hozumi and K. Hashimoto, Design and preparation of a bulk magnet exhibiting an inverted hysteresis loop, Phys. Rev. B, 64 (2001) 132404-1–132404-4.
27. Y. Z. Wu, G. S. Dong and X. F. Jin, Negative magnetic remanence in Co/Mn/Co grown on GaAs (001), Phys. Rev. B, 64 (2001) 214406-1–214406-5.
28. S. Demirtas, M. R. Hossu, M. Arikan, A. R. Koymen and M. B. Salamon, Tunable negative and positive coercivity for SmCo/(Co/Gd) exchange springs investigated with SQUID magnetometry, Phys. Rev. B, 76 (2007) 214430-1–214430-7.
29. W. H. Meiklejohn and C. P. Bean, New magnetic anisotropy, Phy. Rev. 102 (1956) 1413-1414.
30. J. Nogues, D. Lederman, T. J. Moran and I. K. Schuller, Positive exchange bias in FeF_2-Fe bilayers, Phy. Rev. Lett. 76 (1996) 4624-4627.
31. W. H. Meiklejohn, Exchange Anisotropy-A Review, J. Appl. Phy. Suppl, 33 (1962) 1328–1335.
32. H. Singh, R. Gupta, T. Chakraborty, A. Gupta, and C. Mitra, Study of Exchange Bias in All Ferromagnetic Fe/Co Soft/Hard Bilayer, IEEE T. Mag, 50 (2014) 4800204-1–4800204-4.
33. J. Nogues and I. K. Schuller, Exchange bias, J. Mag. Mag. Mater. 192 (1999) 203-232.
34. M. Kiwi, Exchange bias theory, J. Mag. Mag. Mater. 234 (2001) 584-595.
35. A. E. Berkowitz and K. Takano, Exchange anisotropy - a review, J. Mag. Mag. Mater. 200 (1999) 552-570.

36. R. L. Stamps, Mechanisms for exchange bias, J. Phys. D: Appl. Phys. 33 (2000) R247- R268.
37. F. Radu and H. Zabel, Exchange Bias Effect of Ferro-/Antiferromagnetic Heterostructures, in: H. Zabel and S. D. Bader (Eds.), Magnetic heterostructures, advances and perspectives in spinstructures and spintransport, Spr. Trac. Mod. Phys. (2008) 97-184.
38. R. Surla, N. Mitrović, S. Djukić and V. Ibrahimović, Amorphous $Fe_{72}Cu_1V_4Si_{15}B_8$ ribbons as a magneto-impedance sensing element, Serbian J. Elect. Eng. 13 (2016) 381-394.
39. L. Lutterotti, Total pattern fitting for the combined size-strain-stress-texture determination in thin film diffraction, Nucl. Instrum. Meth. B, 268 (2010) 334-340.
40. JCPDS PDF-2 Database, ICDD, PA, USA, 2005.
41. ICSD Inorganic Crystals Structure Database, Release 2014/2, FIZ Karlsruhe, Eggenstein-Leopoldshafen, Germany
42. G. K. Williamson and W. H. Hall, X-ray line broadening from filed aluminium and wolfram, Acta Metall. 1 (1953) 22-31.
43. J. E. Gao, H. X. Li, Z. B. Jiao, Y. Wu, Y. H. Chen, T. Yu and Z. P. Lu, Effects of nanocrystal formation on the soft magnetic properties of Fe-based bulk metallic glasses, App. Phys. Lett. 99 (2011) 052504-1–052504-3.
44. G. Herzer, Grain structure and magnetism of nanocrystalline ferromagnets, IEEE T. Mag. 25 (1989) 3327-3329.
45. G. Herzer, Anisotropies in soft magnetic nanocrystalline alloys, J. Mag. Mag. Mater. 294 (2005) 99-106.

Сажетак: *Ефекат инверзног магнетног хистерезиса и ефекат помераја хистерезисне криве у односу на H=0 осу испитивани су код $Fe_{72}Cu_1V_4Si_{15}B_8$ легуре у облику траке са аморфно-нанокристалном структуром. Након спроведених термичких третмана структура садржи α-Fe(Si), $Fe_{23}B_6$ и Fe_2B нанокристална зрна распоређена у аморфној матрици која су у директној корелацији са магнетним својствима. Промене односа површине и запремине узорка доводе до промене магнетне енергије двофазног система који чине магнетно мека и магнетно полутврда фаза, а самим тим и на изглед криве магнетног хистерезиса. Криве инверзног магнетног хистерезиса су уочене код узорака краћих од 10 mm, док су код дужих узорака регистроване нормалне хистерезисне криве. Код узорка који је одгреван на температури 723 K (а потом охлађени до собне температуре) уочено је померање хистерезисне криве у десно (тзв. позитиван помак, а поље Heb > 0), док је код узорка одгреваног на 823 K, уочено померање хистерезисне криве у лево (тзв. негативан помак, а поље Heb < 0). Позитиван помак хистерезисне криве је најизраженији код узорка одгреваног на 723 K, при чему је код овог узорка регистровано и најмање магнетно поље при којем крива магнетног хистерезиса прелази из инверзног у нормалан смер. Спроведеним истраживањима је експериментално потврђен утицај изменске интеракције двају присутних магнетних фаза (магнетно меке α-Fe(Si) фазе и магнетно полутврде Fe_2B фазе) на испитиване ефекте.*

Кључне речи*: $Fe_{72}Cu_1V_4Si_{15}B_8$ трака, аморфно-нанокристална структура, крива инверзног магнетног хистерезиса, померај хистерезисне криве.*